

# $\beta$ -(Al<sub>x</sub>Ga<sub>1-x</sub>)<sub>2</sub>O<sub>3</sub>/Ga<sub>2</sub>O<sub>3</sub> Tri-Gate MOSHEMT with 70 GHz $f_T$ and 55 GHz $f_{MAX}$

Noor Jahan Nipu, Chinmoy Nath Saha, and Uttam Singisetti, *Senior Member, IEEE*

**Abstract**—We report  $\beta$ -(Al<sub>x</sub>Ga<sub>1-x</sub>)<sub>2</sub>O<sub>3</sub>/Ga<sub>2</sub>O<sub>3</sub> (AlGaO/GaO) tri-gate heterostructure MOSHEMTs incorporating a thin 5 nm Al<sub>2</sub>O<sub>3</sub> gate oxide layer for improved gate control and reduced leakage. The devices were fabricated on AlGaO/GaO heterostructures grown by ozone MBE on Fe-doped Ga<sub>2</sub>O<sub>3</sub> (010) substrates. The tri-gate MOSHEMTs, with 1  $\mu$ m-wide fins and  $L_g$ =155 nm, exhibit a peak current-gain cut-off frequency  $f_T$ =70 GHz and a power-gain cut-off frequency  $f_{MAX}$ =55 GHz. The  $f_T \cdot L_g$  product of 10.85 GHz- $\mu$ m is the highest among reported  $\beta$ -Ga<sub>2</sub>O<sub>3</sub> FETs to date. The devices show  $V_{TH} \approx -0.5$  V, an on/off ratio  $> 10^6$ ,  $I_{ON} = 80$  mA/mm, a peak  $g_m = 60$  mS/mm, and a low gate leakage current of  $\sim 10^{-10}$  mA/mm at  $V_{GS} = 0.5$  V. Passivation with a 100 nm ALD Al<sub>2</sub>O<sub>3</sub> layer effectively removes DC–RF dispersion and maintains stable operation under pulsed I–V and repeated RF measurements. These results demonstrate the potential of tri-gate AlGaO/GaO MOSHEMTs for next-generation high-frequency and high-power applications.

**Index Terms**—Gallium oxide, MOSHEMT, tri-gate, high-frequency devices, passivation, ozone MBE,  $\beta$ -(Al<sub>x</sub>Ga<sub>1-x</sub>)<sub>2</sub>O<sub>3</sub>/Ga<sub>2</sub>O<sub>3</sub>.

## I. INTRODUCTION

$\beta$ -Ga<sub>2</sub>O<sub>3</sub> is an attractive ultra wide band gap (UWBG) semiconductor for power and RF electronics because of its high critical field and good saturation velocity, giving a large Johnson figure of merit [1]–[3]. Multi-kV diodes and FETs already show strong high-voltage capability [4]–[9]. In the  $\beta$ -(Al<sub>x</sub>Ga<sub>1-x</sub>)<sub>2</sub>O<sub>3</sub>/Ga<sub>2</sub>O<sub>3</sub> system, a 2DEG can form at the heterointerface, enabling higher mobility and reduced impurity scattering [10] which has enabled continued improve in RF and breakdown metrics [11]–[16]. In recent years, our group reported AlGaO/GaO HFETs with  $f_T \approx 30$  GHz and thin-channel  $\beta$ -Ga<sub>2</sub>O<sub>3</sub> MOSFETs with  $f_{MAX}=55$  GHz and 5.4 MV/cm breakdown field [17]–[19], stable RF operation up to 250 °C and planar HFETs with  $f_T/f_{MAX} = 32/65$  GHz after Ga<sub>2</sub>O<sub>3</sub> passivation [20], [21].

Conventional HEMTs face large gate leakage, affecting noise, power, and reliability. By adding a gate dielectric helps to reduce these issues, motivating metal-oxide-semiconductor

We acknowledge the support from AFOSR (Air Force Office of Scientific Research) under award FA9550-18-1-0479 (Program Manager: Ali Sayir), from NSF under awards ECCS 2019749, 2231026 from Semiconductor Research Corporation under GRC Task ID 3007.001, and Coherent II-VI Foundation Block Gift Program. This work used the electron beam lithography system acquired through NSF MRI award ECCS 1919798.

All authors are with the Department of Electrical Engineering, University at Buffalo, Buffalo, NY 14260, USA.

high electron mobility transistors (MOSHEMTs) structure [22], [23]. Also, by scaling the gate length  $L_g$ , electrostatic control weakens and short-channel effects increase [24]. Tri-gate/FinFET geometries improve gate control by wrapping the channel from three sides and are effective for power and RF devices [25]–[29]. However, RF tri-gate devices in AlGaO/GaO have not been shown.

This letter demonstrates the first tri-gate  $\beta$ -(Al<sub>0.19</sub>Ga<sub>0.81</sub>)<sub>2</sub>O<sub>3</sub>/Ga<sub>2</sub>O<sub>3</sub> (AlGaO/GaO) MOSHEMTs with a thin Al<sub>2</sub>O<sub>3</sub> gate dielectric and with heavily doped source-drain N++ Ga<sub>2</sub>O<sub>3</sub> regrowth. We report much lower gate current and a positive  $V_{TH}$  shift compared to our planar HFETs. From RF measurement we achieved  $f_T/f_{MAX}$  of 70 GHz/55 GHz and  $f_T \cdot L_g$  product of 10.85 GHz- $\mu$ m which is higher than all previously reported values.

## II. DEVICE STRUCTURE AND FABRICATION

The epitaxial layers were grown on (010) Fe-doped semi-insulating Ga<sub>2</sub>O<sub>3</sub> by ozone MBE following the growth condition of [30]. The stack (Fig.1(a)) consists of 350 nm UID buffer, 4.5 nm Si-doped  $\beta$ -(Al<sub>0.19</sub>Ga<sub>0.81</sub>)<sub>2</sub>O<sub>3</sub>/Ga<sub>2</sub>O<sub>3</sub> ( $3 \times 10^{18}$  cm<sup>-3</sup>), and 22.5 nm UID  $\beta$ -(Al<sub>0.19</sub>Ga<sub>0.81</sub>)<sub>2</sub>O<sub>3</sub>/Ga<sub>2</sub>O<sub>3</sub> barrier.

The early steps follow our previous HFET flow [21]. For source/drain regrowth, we grew a 75 nm highly doped N++ Ga<sub>2</sub>O<sub>3</sub> at 600 °C ( $3 \times 10^{19}$  cm<sup>-3</sup>). After removing the SiO<sub>2</sub>/Al<sub>2</sub>O<sub>3</sub> regrowth mask in buffered HF, the devices were isolated by BCl<sub>3</sub> based ICP/RIE. Fins were patterned by electron beam lithography (EBL) using hydrogen silsesquioxane (HSQ) as etch mask and etched using low-power BCl<sub>3</sub> ICP/RIE. Final fin dimensions are  $h_{fin} \approx 60$  nm,  $w_{fin} \approx 1$   $\mu$ m, with 1  $\mu$ m spacing. After the fin etching, a solvent cleaning was carried out with acetone, isopropanol and DI water to prevent any surface contamination. The source, drain and gate pad contacts (Ti/Au/Ni = 50/120/25 nm) were deposited by e-beam evaporation and annealed at 490°C for 2 min. Before the gate oxide, the surface was cleaned using piranha solution. A 5 nm thin Al<sub>2</sub>O<sub>3</sub> gate dielectric was deposited by thermal ALD at 250°C, followed by Ni/Au (30/180 nm) gate metal. Finally, we passivated the surface with 100 nm Al<sub>2</sub>O<sub>3</sub> by thermal ALD at 300 °C. The final cross-section of the device schematic is shown in Fig.1(b) with magnified SEM and FIB image (Fig.1(c)). The simulated electron density from a self-consistent Schrodinger-Poisson solver using Silvaco TCAD is shown in Fig.1(d). It gave 2DEG density of approximately  $3.5 \times 10^{11}$  cm<sup>-2</sup> [17].

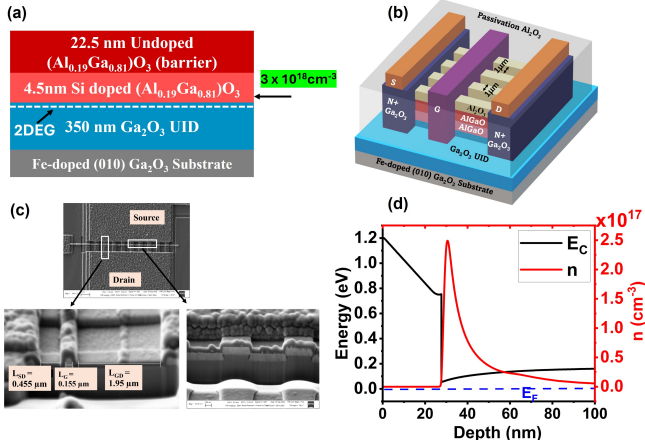


**Fig. 1.** (a) Epitaxial layer stack of tri-gate HFET, (b) Cross-section of final fabricated device structure, (c) Magnified top view SEM image of a fabricated device showing I gate device with dimensions  $L_{SG}/L_G/L_{DG} = 0.455 \mu\text{m}, 0.155 \mu\text{m}, 1.95 \mu\text{m}$  and the FIN cross section. (d) Simulated energy band diagram and electron concentration profile. [17].

### III. RESULTS AND DISCUSSION

We have carried out DC measurements using HP4155B analyzer and then normalized by  $w_{\text{fin}} \times N_{\text{fin}}$ . From TLM on the  $\text{N}^{++}$  through 2DEG path, we extracted  $(R_{C,\text{total}}) = 147.92 \Omega \text{ mm}$  and channel sheet resistance ( $R_{\text{sheet,ch}}$ ) around  $129 \text{ k}\Omega/\square$ , higher than prior reports due to lower doping and 2DEG density [10], [11], [21], [31].

The measured output and transfer curves for a device with  $L_G = 155 \text{ nm}$  are shown in Fig.2(a) and (b). We got  $I_{D,\text{max}} = 80 \text{ mA/mm}$  with  $R_{\text{ON}} = 28.2 \Omega \text{ mm}$  at  $V_{GS} = 1 \text{ V}$  and  $V_{DS} = 5 \text{ V}$ . The lower current is expected because the fin halves the cross-section and adds extra series resistance in the fin pitch; fin etching may also reduce mobility [29]. The device shows peak  $g_m = 60 \text{ mS/mm}$  at  $V_{DS} = 5 \text{ V}$  and  $V_{GS} \approx 0.5 \text{ V}$ , a linearly-extrapolated  $V_{TH} \approx -0.5 \text{ V}$  (Fig.2 (b)), on/off ratio  $\sim 10^6$ , and gate current  $\sim 10^{-10} \text{ mA/mm}$  at  $V_{GS} = 0.5 \text{ V}$  (Fig.2 (c)). Compared to our planar HFETs that pinch off near  $V_{GS} = -6 \text{ V}$  [21], the tri-gate shifts  $V_{TH}$  positively and suppresses short-channel effects such as DIBL.

A low-temperature DC measurement with range of 50 K–400 K, step of 50 K show  $I_{D,\text{max}} \approx 110 \text{ mA/mm}$  at 50 K with  $R_{\text{ON}} = 16 \Omega \text{ mm}$  ( $V_{GS} = 1 \text{ V}$ ,  $V_{DS} = 5 \text{ V}$ ) (Fig.2(d)), which is about 38% higher than at room temperature, consistent with reduced optical-phonon scattering [31]. In Fig.2 (e), peak  $g_m$  at 50 K is  $\sim 73 \text{ mS/mm}$  with no clear  $V_{TH}$  shift from room temperature value.

Before passivation we measured the pulsed IV with Auriga system (not shown here). With gate-lag bias ( $V_{GS,q} = -3 \text{ V}$ ) the drain current drops by  $\sim 31\%$  compared to DC. Under a double-pulse bias ( $V_{GS,q} = -5 \text{ V}$ ,  $V_{DS,q} = 7 \text{ V}$ ) the drop is  $\sim 70\%$ , pointing to traps under the gate and in the gate–drain access, similar to our prior work [19], [20], [32].

After passivation with 100 nm  $\text{Al}_2\text{O}_3$ , the pulse  $I_D$ - $V_{DS}$  is shown in Fig.2(f). At 200 ns pulse width (and even after eight RF runs), we observed no current collapse at both gate pulse ( $V_{GS,q} = -2 \text{ V}$ ) and dual pulse condition ( $V_{GS,q} = -2 \text{ V}$ ,  $V_{DS,q} = 5 \text{ V}$ ). The effect of thicker passivation on  $\beta\text{-Ga}_2\text{O}_3$  FINFETs has

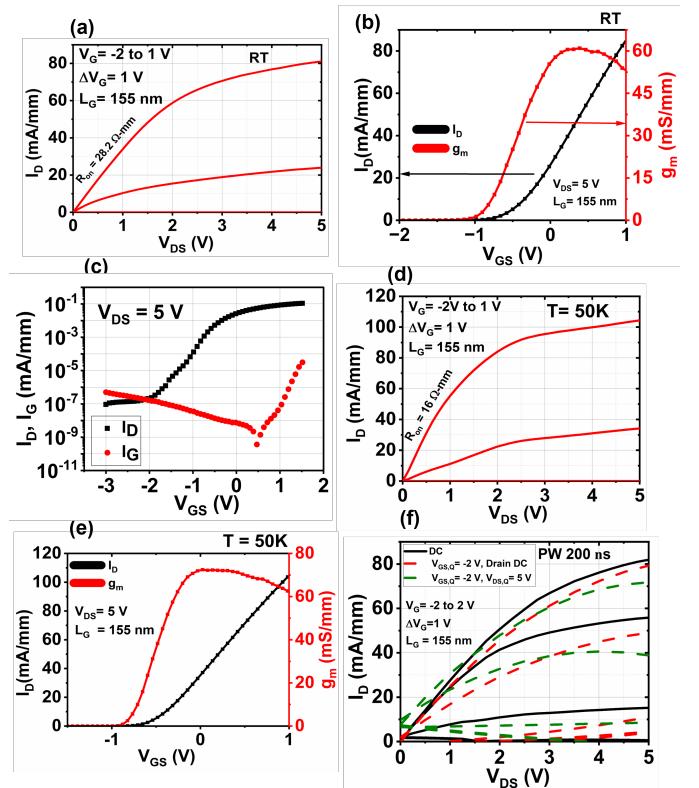


**Fig. 2.** (a)  $I_D$ - $V_{DS}$  output curve at room temperature showing peak  $I_D = 80 \text{ mA/mm}$  with  $R_{\text{ON}} = 28.2 \Omega \text{ mm}$  at  $V_{GS} = 1 \text{ V}$  and  $V_{DS} = 5 \text{ V}$ , (b)  $I_D$ - $V_{GS}$  transfer curve showing peak  $g_m = 60 \text{ mS/mm}$ , (c) Semilog transfer curve showing  $I_D$  and  $I_g$  showing gate leakage current lower  $10^{-10} \text{ mA/mm}$  at  $V_{GS} = 0.5 \text{ V}$  (d) Output curve at  $T = 50 \text{ K}$  showing peak  $I_D = 110 \text{ mA/mm}$  with  $R_{\text{ON}} = 16 \Omega \text{ mm}$  at  $V_{GS} = 1 \text{ V}$  (e)  $I_D$ - $V_{GS}$  transfer curve at  $T = 50 \text{ K}$  showing peak  $g_m \approx 80 \text{ mS/mm}$ , (f) Pulsed  $I_D$ - $V_{DS}$  measurements after 100 nm  $\text{Al}_2\text{O}_3$  passivation (and repeated RF tests): no current collapse for  $V_{GS} = -2 \text{ V}$  and for the double-pulse case  $V_{GS,Q} = -2 \text{ V}$ ,  $V_{DS,Q} = 5 \text{ V}$ , indicating effective trap passivation on fin sidewalls and surface.

not been explored yet. Along with the trap passivation that we have achieved in planar HFET [21], we also achieved strong stabilization which we attribute to conformal passivation of fin sidewalls and the 5 nm gate oxide that lowers gate-leakage-induced trapping. Similar improvement from  $\text{Al}_2\text{O}_3$  dielectrics in fin devices has been reported in  $\text{AlGaN}/\text{GaN}$  [33].

Small-signal S-parameters were measured with an ENA-5071C (100 MHz–20 GHz) using GSG probes. An on-wafer isolated open-pad structure was used for de-embedding [34]. Fig.3(a) and (b) plot short circuit current gain ( $h_{21}$ ), unilateral current gain ( $U$ ), and MAG/MSG and extrapolated them to 0 dB at  $V_{GS} = 1 \text{ V}$  and  $V_{DS} = 15 \text{ V}$ . The device with  $L_G = 0.155 \mu\text{m}$ , yields  $f_T = 70 \text{ GHz}$  and  $f_{\text{MAX}} = 55 \text{ GHz}$ . The  $f_T \cdot L_G$  product is  $10.85 \text{ GHz} \cdot \mu\text{m}$ , the best reported for  $\beta\text{-Ga}_2\text{O}_3$  RF devices. Prior tri-gate  $\beta\text{-Ga}_2\text{O}_3$  reports also show RF improvement over planar devices [29]; here the heterostructure 2DEG further boosts  $g_m$  while the tri-gate provides stronger electrostatic control and reduces short-channel effects, leading to higher current gain and improved frequency response. Fig.3(a) inset shows simplified small signal model of the transistor, simulated using Advanced Design System (ADS), where we use measured  $g_m$ , extracted  $R_i/R_{DS}$  (from z-parameters at 2 GHz), and  $C_{GS}$  is calculated using a geometrical device dimension

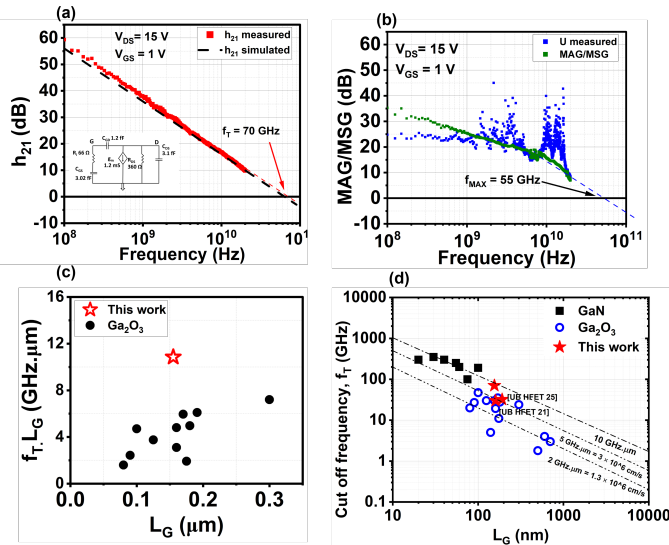


**Fig. 3.** Small-signal RF performance at  $V_{GS}=1$  V and  $V_{DS}=15$  V for  $L_G=0.155$   $\mu\text{m}$  (a) Measured and simulated  $h_{21}$  versus frequency showing  $f_T=70$  GHz. Inset: RF small signal model developed in ADS, with measured  $g_m$  and  $C_{GS}$  adjusted within 30%. (b) Measured unilateral power gain ( $U$ ) and MAG/MSG versus frequency showing  $f_{MAX}=55$  GHz. (c)  $f_T \cdot L_G$  product with  $L_G$  compared with other reported  $\beta\text{-Ga}_2\text{O}_3$  FETs, showing the highest  $f_T \cdot L_G$  product (10.85 GHz· $\mu\text{m}$ ) achieved in this work. (d)  $f_T$  versus  $L_G$  benchmark plot of our devices compared to other  $\beta\text{-Ga}_2\text{O}_3$  RF FETs and AlGaN/GaN HEMTs.

of 2 finger width, assuming the device is unilateral. As seen in the Fig.3(a), we got a good fit between measured and simulated data. Here we had to vary the parameters within 30% accuracy range to match the measured data which is well within a desired fit. A T-gate and reduced access resistance should increase  $f_{MAX}$ .

It also shows the benchmark plot comparison of our FET with other  $\beta\text{-Ga}_2\text{O}_3$  RF FETs which shows that our calculated  $f_T \cdot L_G$  product is the highest values reported for  $\beta\text{-Ga}_2\text{O}_3$  FETs (Fig.3(c)). Fig.3(d) shows the variation of  $f_T$  with  $L_G$  for different GaN and  $\beta\text{-Ga}_2\text{O}_3$  FETs. The value of  $f_T \cdot L_G$  product corresponds to  $V_{sat}$  approximately  $3 \times 10^6$  cm/s demonstrating excellent high-frequency performance, comparable to state-of-the-art GaN RF transistors.

#### IV. CONCLUSION

We demonstrated tri-gate AlGaO/GaO HFETs with  $f_T=70$  GHz and  $f_{MAX}=55$  GHz at  $L_G$  155 nm, giving a record  $f_T \cdot L_G = 10.85$  GHz· $\mu\text{m}$  for  $\beta\text{-Ga}_2\text{O}_3$  FETs. The devices show  $V_{TH} \approx 0.5$  V, an on/off ratio  $>10^6$ , and a low gate leakage current of  $\sim 10^{-10}$  mA/mm. A 100 nm  $\text{Al}_2\text{O}_3$  passivation removes DC–RF dispersion and keeps the RF stable. The results point to tri-gate AlGaO/GaO as a strong platform for next-generation RF power electronics.

#### REFERENCES

- A. J. Green, J. Speck, G. Xing, P. Moens, F. Allerstam, K. Gummelius, T. Neyer, A. Arias-Purdue, V. Mehrotra, A. Kuramata *et al.*, “ $\beta$ -Gallium oxide power electronics,” *APL Materials*, vol. 10, no. 2, p. 029201, 2022.
- A. J. Green, K. D. Chabak, E. R. Heller, R. C. Fitch, M. Baldini, A. Fiedler, K. Irmischer, G. Wagner, Z. Galazka, S. E. Tetlak, A. Crespo, K. Leedy, and G. H. Jessen, “3.8-MV/cm breakdown strength of MOVPE-grown Sn-doped  $\beta\text{-Ga}_2\text{O}_3$  MOSFETs,” *IEEE Electron Device Letters*, vol. 37, no. 7, pp. 902–905, 2016.
- K. Ghosh and U. Singisetti, “Ab initio velocity-field curves in monoclinic  $\beta\text{-Ga}_2\text{O}_3$ ,” *Journal of Applied Physics*, vol. 122, no. 3, p. 035702, 2017.
- E. Farzana, F. Alema, W. Y. Ho, A. Mauze, T. Itoh, A. Osinsky, and J. S. Speck, “Vertical  $\beta\text{-Ga}_2\text{O}_3$  field plate schottky barrier diode from metal-organic chemical vapor deposition,” *Applied Physics Letters*, vol. 118, no. 16, p. 162109, 2021.
- D. H. Mudiyanselage, D. Wang, and H. Fu, “Wide bandgap vertical kv-class  $\beta\text{-Ga}_2\text{O}_3/\text{GaN}$  heterojunction pn power diodes with mesa edge termination,” *IEEE Journal of the Electron Devices Society*, vol. 10, pp. 89–97, 2021.
- C. Wang, Q. Yan, C. Zhang, C. Su, K. Zhang, S. Sun, Z. Liu, W. Zhang, S. Alghamdi, E. Ghandourah *et al.*, “ $\beta\text{-Ga}_2\text{O}_3$  lateral schottky barrier diodes with  $\sim 10$  kV breakdown voltage and anode engineering,” *IEEE Electron Device Letters*, 2023.
- A. Bhattacharyya, S. Roy, P. Ranga, C. Peterson, and S. Krishnamoorthy, “High-Mobility Tri-gate  $\beta\text{-Ga}_2\text{O}_3$  MESFETs with a power figure of merit over  $0.9 \text{ GW/cm}^2$ ,” *IEEE Electron Device Letters*, vol. 43, no. 10, pp. 1637–1640, 2022.
- N. K. Kalarickal, Z. Xia, H.-L. Huang, W. Moore, Y. Liu, M. Brenner, J. Hwang, and S. Rajan, “ $\beta\text{-}(\text{Al}_{0.18}\text{Ga}_{0.82})_2\text{O}_3$  double heterojunction transistor with average field of 5.5 MV/cm,” *IEEE Electron Device Letters*, vol. 42, no. 6, pp. 899–902, 2021.
- D. M. Dryden, K. J. Liddy, A. E. Islam, J. C. Williams, D. E. Walker, N. S. Hendricks, N. A. Moser, A. Arias-Purdue, N. P. Sepelak, K. DeLollo *et al.*, “Scaled t-gate  $\beta\text{-Ga}_2\text{O}_3$  mesfets with 2.45 kv breakdown and high switching figure of merit,” *IEEE Electron Device Letters*, vol. 43, no. 8, pp. 1307–1310, 2022.
- S. Krishnamoorthy, Z. Xia, C. Joishi, Y. Zhang, J. McGlone, J. Johnson, M. Brenner, A. R. Arehart, J. Hwang, S. Lodha *et al.*, “Modulation-doped  $\beta\text{-}(\text{Al}_{0.2}\text{Ga}_{0.8})_2/\text{Ga}_2\text{O}_3$  field-effect transistor,” *Applied Physics Letters*, vol. 111, no. 2, 2017.
- Y. Zhang, A. Neal, Z. Xia, C. Joishi, J. M. Johnson, Y. Zheng, S. Bajaj, M. Brenner, D. Dorsey, K. Chabak *et al.*, “Demonstration of high mobility and quantum transport in modulation-doped  $\beta\text{-}(\text{Al}_{x}\text{Ga}_{1-x})_2\text{Ga}_2\text{O}_3$  heterostructures,” *Applied Physics Letters*, vol. 112, no. 17, 2018.
- Z. Xia, H. Xue, C. Joishi, J. McGlone, N. K. Kalarickal, S. H. Sohel, M. Brenner, A. Arehart, S. Ringel, S. Lodha, W. Lu, and S. Rajan, “ $\beta\text{-}\text{Ga}_2\text{O}_3$  delta-doped field-effect transistors with current gain cutoff frequency of 27 ghz,” *IEEE Electron Device Letters*, vol. 40, no. 7, pp. 1052–1055, 2019.
- M. Zhou, H. Zhou, S. Huang, M. Si, Y. Zhang, T. Luan, H. Yue, K. Dang, C. Wang, Z. Liu *et al.*, “1.1 a/mm  $\beta\text{-Ga}_2\text{O}_3$  on 3-on-sic rf mosfets with 2.3 w/mm  $p_{out}$  and 30% pae at 2 ghz and f t/f max of 27.6/57 ghz,” in *2023 International Electron Devices Meeting (IEDM)*. IEEE, 2023, pp. 1–4.
- M. Zhou, H. Zhou, S. Mengwei, G. Gao, X. Chen, X. Zhu, K. Dang, M. Peijun, M. Xiaohua, X. Zheng *et al.*, “71 ghz- $f_{max}$   $\beta\text{-Ga}_2\text{O}_3$  on sic rf power mosfets with record  $p_{out} = 3.1 \text{ w/mm}$  and pae=50.8% at 2 ghz,  $p_{out} = 2.3 \text{ w/mm}$  at 4 ghz, and low microwave noise figure,” in *2024 IEEE Symposium on VLSI Technology and Circuits (VLSI Technology and Circuits)*. IEEE, 2024, pp. 1–2.
- X. Yu, W. Xu, Y. Wang, B. Qiao, R. Shen, J. Zhou, Z. Li, T. You, Z. Shen, K. Zhang *et al.*, “Heterointegrated  $\beta\text{-Ga}_2\text{O}_3$ -on-sic rf mosfets with  $f_T/f_{MAX}$  of 47/51 ghz by ion-cutting process,” *IEEE Electron Device Letters*, 2023.
- M. Zhou, H. Zhou, S. Alghamdi, G. Gao, X. Liu, M. Xiang, X. Chen, Z. Liu, S. Wasly, Y. Hao, and J. Zhang, “C-band  $\beta\text{-Ga}_2\text{O}_3$ -on-sic rf power mosfets with high output power density and low microwave noise figure,” *IEEE Transactions on Electron Devices*, vol. 72, no. 6, pp. 2874–2878, 2025.
- A. Vaidya, C. N. Saha, and U. Singisetti, “Enhancement mode  $\beta\text{-}(\text{Al}_x\text{Ga}_{1-x})_2\text{O}_3/\text{Ga}_2\text{O}_3$  heterostructure FET (HFET) with high transconductance and cutoff frequency,” *IEEE Electron Device Letters*, vol. 42, no. 10, pp. 1444–1447, 2021.
- C. N. Saha, A. Vaidya, N. J. Nipu, L. Meng, D. S. Yu, H. Zhao, and U. Singisetti, “Thin channel  $\text{Ga}_2\text{O}_3$  MOSFET with 55 GHz fmax and  $\sim 100$  V breakdown,” *Applied Physics Letters*, vol. 125, no. 6, 2024.
- C. N. Saha, A. Vaidya, A. F. M. A. U. Bhuiyan, L. Meng, S. Sharma, H. Zhao, and U. Singisetti, “Scaled  $\beta\text{-Ga}_2\text{O}_3$  thin channel MOSFET with 5.4 MV/cm average breakdown field and near 50 GHz  $f_{MAX}$ ,”

*Applied Physics Letters*, vol. 122, no. 18, p. 182106, 2023. [Online]. Available: <https://doi.org/10.1063/5.0149062>

[20] C. N. Saha, A. Vaidya, and U. Singisetti, "Temperature dependent pulsed IV and RF characterization of  $\beta$ -(Al<sub>x</sub>Ga<sub>1-x</sub>)<sub>2</sub>O<sub>3</sub>/Ga<sub>2</sub>O<sub>3</sub> hetero-structure FET with ex situ passivation," *Applied Physics Letters*, vol. 120, no. 17, p. 172102, 2022.

[21] C. N. Saha, N. J. Nipu, and U. Singisetti, "High performance vacuum annealed  $\beta$ -(al<sub>x</sub>ga<sub>1-x</sub>)<sub>2</sub>o<sub>3</sub>/ga<sub>2</sub>o<sub>3</sub> h fet with ft/fmax of 32/65 ghz," *Applied Physics Express*, 2025.

[22] A. Khodabakhsh, A. Amini, and R. Faraji, "Tandem evaluation of aln/ $\beta$ - and  $\varepsilon$ -ga<sub>2</sub>o<sub>3</sub> tri-gate moshemts," *IEEE Transactions on Electron Devices*, vol. 72, no. 7, pp. 3452–3460, 2025.

[23] K.-S. Im, H.-S. Kang, J.-H. Lee, S.-J. Chang, S. Cristoloveanu, M. Bawedin, and J.-H. Lee, "Characteristics of gan and algan/gan finfets," *Solid-state electronics*, vol. 97, pp. 66–75, 2014.

[24] G. H. Jessen, R. C. Fitch, J. K. Gillespie, G. Via, A. Crespo, D. Langley, D. J. Denninghoff, M. Trejo, and E. R. Heller, "Short-channel effect limitations on high-frequency operation of algan/gan hemts for t-gate devices," *IEEE Transactions on Electron Devices*, vol. 54, no. 10, pp. 2589–2597, 2007.

[25] E. Ture, P. Brückner, F. V. Raay, R. Quay, O. Ambacher, M. Alsharef, R. Granzner, and F. Schwierz, "Performance and parasitic analysis of sub-micron scaled tri-gate algan/gan hemt design," in *2015 10th European Microwave Integrated Circuits Conference (EuMIC)*, 2015, pp. 97–100.

[26] A. Bhattacharyya, S. Roy, P. Ranga, C. Peterson, and S. Krishnamoorthy, "High-mobility tri-gate  $\beta$ -ga<sub>2</sub>o<sub>3</sub> mesfets with a power figure of merit over 0.9 gw/cm<sup>2</sup>," *IEEE Electron Device Letters*, vol. 43, no. 10, pp. 1637–1640, 2022.

[27] Z. Wang, S. Kumar, T. Kamimura, H. Murakami, Y. Kumagai, and M. Higashiwaki, "Ga<sub>2</sub>O<sub>3</sub> fin field-effect transistors with on-axis (100)-plane gate sidewalls fabricated on ga<sub>2</sub>o<sub>3</sub> (010) substrates," *Japanese Journal of Applied Physics*, vol. 63, no. 10, p. 100902, 2024.

[28] Y. Zhang, A. Mauze, F. Alema, A. Osinsky, T. Itoh, and J. S. Speck, " $\beta$ -ga<sub>2</sub>o<sub>3</sub> lateral transistors with high aspect ratio fin-shape channels," *Japanese Journal of Applied Physics*, vol. 60, no. 1, p. 014001, 2020.

[29] X. Yu, H. Gong, J. Zhou, Z. Shen, F.-f. Ren, D. Chen, X. Ou, Y. Kong, Z. Li, T. Chen *et al.*, "Rf performance enhancement in sub- $\mu$ m scaled  $\beta$ -ga<sub>2</sub>o<sub>3</sub> tri-gate finfets," *Applied Physics Letters*, vol. 121, no. 7, 2022.

[30] A. Vaidya, J. Sarker, Y. Zhang, L. Lubecki, J. Wallace, J. D. Poplawsky, K. Sasaki, A. Kuramata, A. Goyal, J. A. Gardella *et al.*, "Structural, band and electrical characterization of  $\beta$ -(al0.19ga0.81)2o<sub>3</sub> films grown by molecular beam epitaxy on sn doped  $\beta$ -ga<sub>2</sub>o<sub>3</sub> substrate," *Journal of Applied Physics*, vol. 126, no. 9, 2019.

[31] Y. Zhang, Z. Xia, J. McGlone, W. Sun, C. Joishi, A. R. Arehart, S. A. Ringel, and S. Rajan, "Evaluation of low-temperature saturation velocity in  $\beta$ -(al<sub>x</sub>ga<sub>1-x</sub>)<sub>2</sub>o<sub>3</sub>/ga<sub>2</sub>o<sub>3</sub> modulation-doped field-effect transistors," *IEEE Transactions on Electron Devices*, vol. 66, no. 3, pp. 1574–1578, 2019.

[32] A. Vaidya and U. Singisetti, "Temperature-dependent current dispersion study in  $\beta$ -Ga<sub>2</sub>O<sub>3</sub> fets using sub-microsecond pulsed i–v characteristics," *IEEE Transactions on Electron Devices*, vol. 68, no. 8, pp. 3755–3761, 2021.

[33] X. Zhou, X. Tan, Y. Lv, Y. Wang, X. Song, G. Gu, P. Xu, H. Guo, Z. Feng, and S. Cai, "Dynamic characteristics of algan/gan fin-mishemts with al<sub>2</sub>o<sub>3</sub> dielectric," *IEEE Transactions on Electron Devices*, vol. 65, no. 3, pp. 928–935, 2018.

[34] M. C. A. M. Koolen, J. A. M. Geelen, and M. P. J. G. Versleijen, "An improved de-embedding technique for on-wafer high-frequency characterization," in *Proc. Bipolar Circuits and Technology Meeting (BCTM)*, Minneapolis, MN, USA, 1991, pp. 188–191.